



HAL
open science

A Thickened-Hole Model for Large Eddy Simulations over Multiperforated Liners

R. Bizzari, D. Lahbib, A. Dauplain, F. Duchaine, L. Gicquel, Franck Nicoud

► **To cite this version:**

R. Bizzari, D. Lahbib, A. Dauplain, F. Duchaine, L. Gicquel, et al.. A Thickened-Hole Model for Large Eddy Simulations over Multiperforated Liners. *Flow, Turbulence and Combustion*, 2018, 101 (3), pp.705-717. 10.1007/s10494-018-9909-3 . hal-02049186

HAL Id: hal-02049186

<https://hal.science/hal-02049186>

Submitted on 27 Feb 2019

HAL is a multi-disciplinary open access archive for the deposit and dissemination of scientific research documents, whether they are published or not. The documents may come from teaching and research institutions in France or abroad, or from public or private research centers.

L'archive ouverte pluridisciplinaire **HAL**, est destinée au dépôt et à la diffusion de documents scientifiques de niveau recherche, publiés ou non, émanant des établissements d'enseignement et de recherche français ou étrangers, des laboratoires publics ou privés.

A Thickened-Hole Model for Large Eddy Simulations over Multiperforated Liners

R. Bizzari¹  · D. Lahbib¹ · A. Dauplain¹ ·
F. Duchaine¹ · L. Y. M. Gicquel¹ · F. Nicoud²

Abstract In aero-engines, multiperforation cooling systems are often used to shield the combustor wall and ensure durability of the engine. Fresh air coming from the casing goes through thousands of angled perforations and forms a film which protects the liner. When performing Large Eddy Simulations (LES) of a real engine, the number of sub-millimetric holes is far too large to allow a complete and accurate description of each aperture. Homogeneous models allow to simulate multiperforated plates with a mesh size bigger than the hole but fail in representing the jet penetration and mixing. A heterogeneous approach is proposed in this study, where the apertures are thickened if necessary so that the jet-crossflow interaction is properly represented. Simulations using homogeneous and thickened-hole models are compared to a fully resolved computation for various grid resolutions in order to illustrate the potential of the method.

Keywords Aerodynamics · LES · Multiperforated plate · Modelling

1 Introduction

By increasing the compressor pressure ratio, manufacturers have successfully improved the efficiency of the thermodynamic cycle used in aeronautical gas turbines [1]. In parallel, new techniques used to reduce pollutants like the Rich-Burn, Quick-Mix, Lean-Burn (RQL [2]) imposed a drastic reduction of the amount of air available for the cooling of the combustor. The price to pay for these improvements is a higher thermal constraint on the walls of the combustion chamber. Indeed, hot gases can reach up to 2400K when the steel used in the conception cannot sustain more than 1200K. In this context, optimizing the cooling devices

✉ R. Bizzari
romain.bizzari@cerfacs.fr

¹ CERFACS, 42, Av. Gaspard Coriolis, Toulouse 31057 Cedex 1, France

² IMAG, Univ Montpellier, CNRS, Montpellier, France

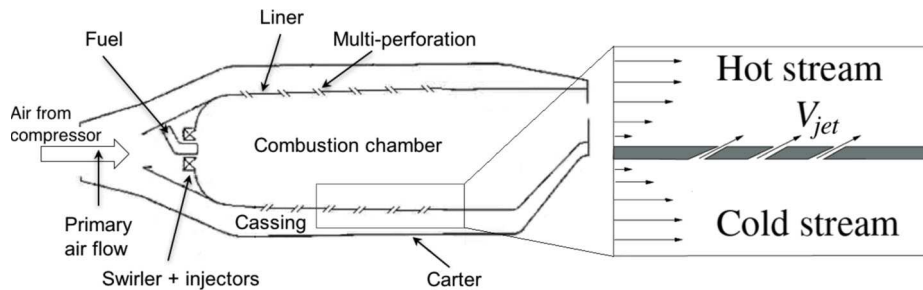


Fig. 1 Principle of effusion cooling. Left: sketch of a combustor where the perforated plate separates the casing from the combustion chamber. Right: flow organization around a perforated plate

becomes a priority [3]. In modern combustors, effusion cooling [4], Fig. 1, is often used for its efficiency, compacity and lightness. During their manufacturing, the liners are laser drilled [5] by thousands of holes with a diameter lower than 0.5 mm. Due to the pressure difference between the casing and the combustor chamber, a micro-jet is formed at each aperture of the perforated plate. These micro-jets interact together and form a consistent film which interacts and mixes with the hot gases from the combustion chamber.

The cooling efficiency is controlled by few parameters: the hole-to-hole distances (Δx , Δz) studied in [6–8], the perforation diameter (d) and α the angle between the plate and the perforation direction explicated on Fig. 2 and studied in [9–12]. These geometric

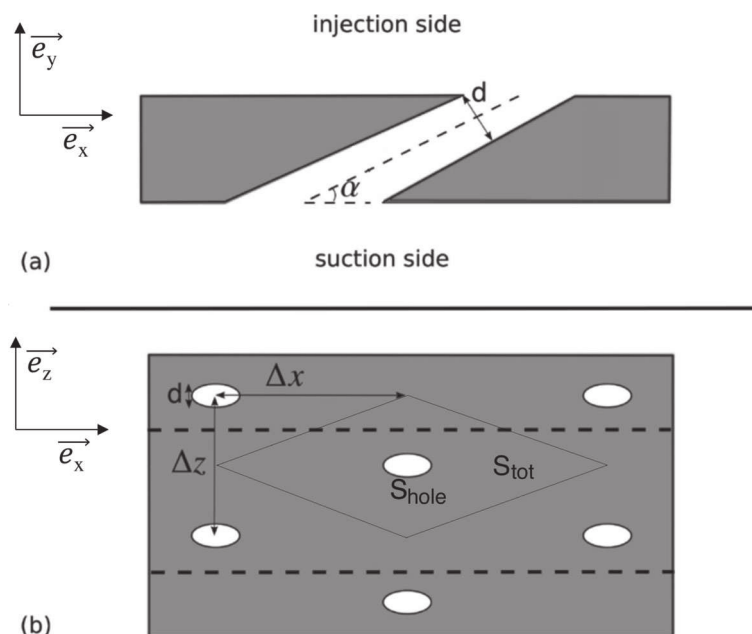


Fig. 2 a Cut of a hole. b Upside view of the plate

parameters yield the plate porosity σ , which represents the ratio of the drilled surface (S_{hole}) compared to the total surface (S_{tot}) delimited by the diamond pattern visible on Fig. 2.

$$\sigma = \frac{S_{hole}}{S_{tot}} = \frac{\pi d^2}{4 \sin(\alpha) \Delta x \Delta z}. \quad (1)$$

Typical values of σ for aeronautical applications are in the range [0.02–0.06]. When performing numerical simulations of combustor, for the fluid solver, Reynolds Average Navier Stokes (RANS) and Large Eddy Simulation (LES) methods can be used. The first one, less expensive, leads to average solutions when the second gives access to instantaneous solutions and thus, better predicts the mixing and the turbulence flame interaction, which is more desirable in combustor simulations. To represent the liners, various modelling strategies have been used in the literature [13–18]. To distinguish these models and relate them to corresponding mesh resolution constraints, it is useful to introduce the aperture-to-mesh ratio:

$$R = \frac{d}{dx}, \quad (2)$$

where d is the diameter of the perforations and dx the typical mesh size. To give an order of magnitude, a coarse mesh would correspond to $R \leq 1$ while a simulation can be considered reasonably well resolved when $R \geq 10$ (even if this specific values is only an approximation and more cells could be needed to resolved the jet in cross flow as mentioned by Mendez and Nicoud [19]). Typical values of R are illustrated on Fig. 3.

When $R \geq 10$, the actual geometry, including effusion pipe, can be reasonably computed and the effect of the multi-perforated liner is obtained by simply using the flow equations. This kind of simulation has been carried out with RANS solvers [20] but is not expected with LES solvers before 20 years for a computational cost reason [21]. At the opposite, when $R \leq 1$, the liner must be represented as a homogeneous surface; apertures are not represented. In this case, either both injection and suction sides can be computed or just the injection side. In both cases, the state-of-the-art is then to use the homogeneous model of Mendez and Nicoud [16] where the coolant flux is homogeneously injected on the whole boundary. This model has indeed proven reliable in many configurations [22]. Its drawbacks are however a bad prediction of the mixing process close to the wall and no benefit from better mesh resolution.

Thanks to the increasing available computational resources, typical mesh resolutions used for industrial LES predictions of actual burners already reach R above unity near the wall and are a clear asset to improve the near wall mixing in a LES context. This however goes with a modelling effort since the homogeneous formulation cannot benefit from such improved resolutions. This approach should then be replaced by a better one, based on a heterogeneous formulation as detailed thereafter.

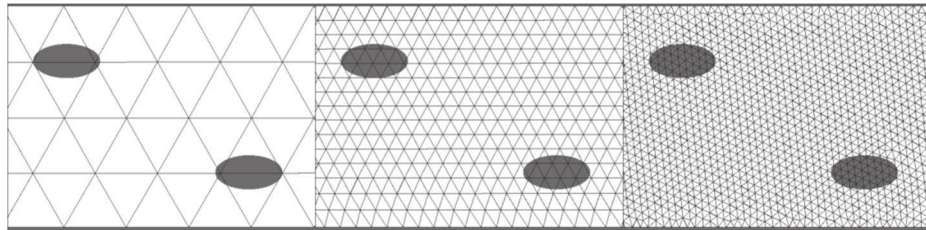


Fig. 3 Projection of multiperforation holes over different grids. Left: $R = 0.5$. Middle: $R = 2$. Right: $R = 4$

In this paper, a new model is proposed and validated. It is based on heterogeneous approach where holes are projected on the mesh. This approach, called thickened-hole model is presented in Section 2. The model is then validated on the Maveric-H configuration representative of aeronautical engines, described in Section 3. In Section 4, the results for a variety of R ratios are examined and compared to a computation performed with the homogeneous model and a resolved computation *ie* hot and cold sides as well as perforations simulated.

2 Multiperforated Plate Models

The thickened-hole model builds partly upon the homogeneous model, the latest is first described in Section 2.1. After that, the thickened-hole model is presented in Section 2.2.

2.1 The homogeneous model

The homogeneous approach models the multiperforated plate as a porous plate injecting mass over its whole surface with a uniform velocity. Mendez and Nicoud [19] showed that a multiperforated plate model must represent the proper mass and longitudinal momentum fluxes across the boundary. These two quantities can be written as:

$$\int_{S_{tot}} \rho V_n^{mod}(x, z) dS = \int_{S_{tot}} \rho V_n^{jet}(x, z) dS, \quad (3)$$

$$\int_{S_{tot}} \rho V_n^{mod}(x, z) V_t^{mod}(x, z) dS = \int_{S_{tot}} \rho V_n^{jet}(x, z) V_t^{jet}(x, z) dS, \quad (4)$$

with ρ the density of the fluid. $V_n^{mod}(x, z)$ and $V_t^{mod}(x, z)$ are respectively the normal and tangential velocity imposed by the homogeneous model on the plate at the position (x, z) . $V_n^{jet}(x, z)$ and $V_t^{jet}(x, z)$ are respectively the normal and tangential velocity at the outlet of the hole for the real pipe at the position (x, z) . When integrated over the control surface S_{tot} , diamond pattern visible on Fig. 2, Eqs. 3 and 4 become:

$$\rho \langle V_n^{mod} \rangle_{S_{tot}} = \rho \langle V_n^{jet} \rangle_{S_{hole}}, \quad (5)$$

$$\rho \langle V_n^{mod} \rangle \langle V_t^{mod} \rangle_{S_{tot}} = \rho \langle V_n^{jet} \rangle \langle V_t^{jet} \rangle_{S_{hole}}, \quad (6)$$

with $\langle \rangle$ the associated mean surface value. It follows that the proper velocity to impose for a homogeneous description of a multiperforated liner is:

$$\langle V_n^{mod} \rangle = \langle V_n^{jet} \rangle / \sigma, \quad (7)$$

$$\langle V_t^{mod} \rangle = \langle V_t^{jet} \rangle, \quad (8)$$

2.2 The thickened-hole model

The homogeneous model allows to represent the main effects of the effusion (proper injected mass and momentum flux), as detailed in [19]. At the same time, representing the heterogeneity of the injection through discrete holes would be beneficial in LES where macro mixing plays a key role. Since typical mesh resolutions are not sufficient to represent the intra jet flow, a basic idea is to make the apertures thicker so that the grid resolution can

represent the modified holes. From the analysis of Mendez and Nicoud [16], (who considered infinitely thickened-holes in a sense), thickening the aperture modifies the momentum flux and must be compensated.

The next step is then to limit the Mendez and Nicoud [16] formulation (7, 8) to the region corresponding to each thickened-hole. Outside of this region, a wall law model, suitable for an impermeable solid plate, is applied. It uses a two layer logarithmic law along with a slip condition applied as detailed in [23]. The injection region of the hole whose center is (x_0, z_0) and whose diameter is d is defined thanks to a distribution function $f(x, z)$, equal to unity in the hole region and zero outside (see Fig. 4):

$$f(x, z) = 0.5 \left(1 - \tanh \left(\frac{\sqrt{(x - x_0)^2 + (z - z_0)^2} - 0.5d\Gamma}{\beta dx} \right) \right). \quad (9)$$

In Eq. 9, Γ is the thickening factor, defined as $\Gamma = \text{Max} \left(\frac{E}{R}, 1 \right)$, where E is the minimum number of cells per hole diameter, defined by the user. The parameter β is introduced to control the stiffness of the distribution function and avoid numerical stability issues. It is also user-defined. Preliminary experiences points to $E = 3$ and $\beta = 0.1$ to be adequate values.

A numerical porosity is then introduced as:

$$\sigma_n = \frac{S_{hole}}{S_{num}} = \frac{S_{hole}}{\int_{S_{tot}} f(x, z) dS}, \quad (10)$$

where S_{num} corresponds to the injection surface, that is equal to the surface of the thickened-hole through which the jet velocity profile is imposed; σ_n is local and associated to each hole. It ranges between 1 when the hole is perfectly represented and σ , the physical porosity used in [16], when coolant air is injected on the whole plate in a homogeneous way. When using the thickened-hole model, the velocity applied on the boundary, noted $V_n^{thick}(x, z)$ and $V_t^{thick}(x, z)$ for the normal and tangential directions respectively, follow the expressions:

$$V_n^{thick}(x, z) = A_n f(x, z), \quad (11)$$

$$V_t^{thick}(x, z) = A_t f(x, z), \quad (12)$$

where $f(x, y)$ introduced the spatial heterogeneity. A_n and A_t are constant values and are determined by the following equations. The mass conservation corresponding to the integration of the normal velocity on the control surface S_{tot} for the thicken hole and for the real jet through the plate allows to find A_n :

$$\int_{S_{tot}} \rho A_n f(x, z) dS = \int_{S_{tot}} \rho V_n^{jet}(x, z) dS, \quad (13)$$

$$A_n = \frac{\langle V_n^{jet} \rangle S_{hole}}{\int_{S_{tot}} f(x, z) dS}, \quad (14)$$

Momentum conservation then allows to find A_t :

$$\int_{S_{tot}} \rho A_n f(x, z) A_t f(x, z) dS = \int_{S_{tot}} \rho V_n^{jet}(x, z) V_t^{jet}(x, z) dS, \quad (15)$$

$$A_t = \langle V_t^{jet} \rangle \frac{\int_{S_{tot}} f(x, z) dS}{\int_{S_{tot}} f^2(x, z) dS}. \quad (16)$$

When the mesh resolution is enough to properly represent the velocity field inside the hole, $R > E$, this model is equivalent to a heterogeneous model without thickening. If $R < E$ apertures are thickened (See Fig. 4). Finally, when $R \ll E$ the model degenerates

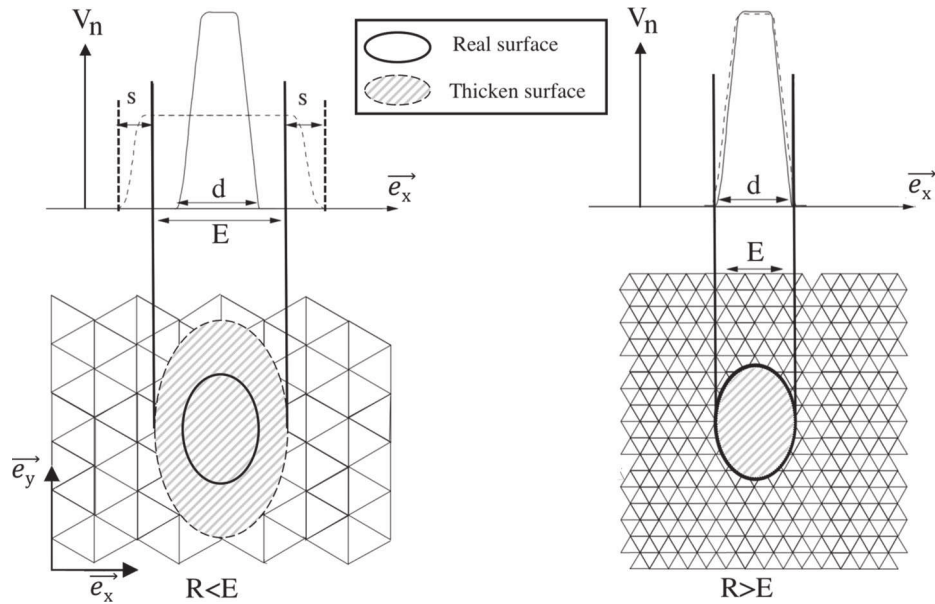


Fig. 4 1D representation of the normal velocity profile (top figures) and representation on a 2D mesh of the injecting surface (bottom figures) for $R = 2$ (left) and $R = 4$ (right)

to a homogeneous model. Note that no turbulence activity or equivalently turbulence shear stress is added on the injection surface of the boundary. Indeed it would be complex to add such terms since the jet size is variable (injection surface S_{num} depends on the thickening)

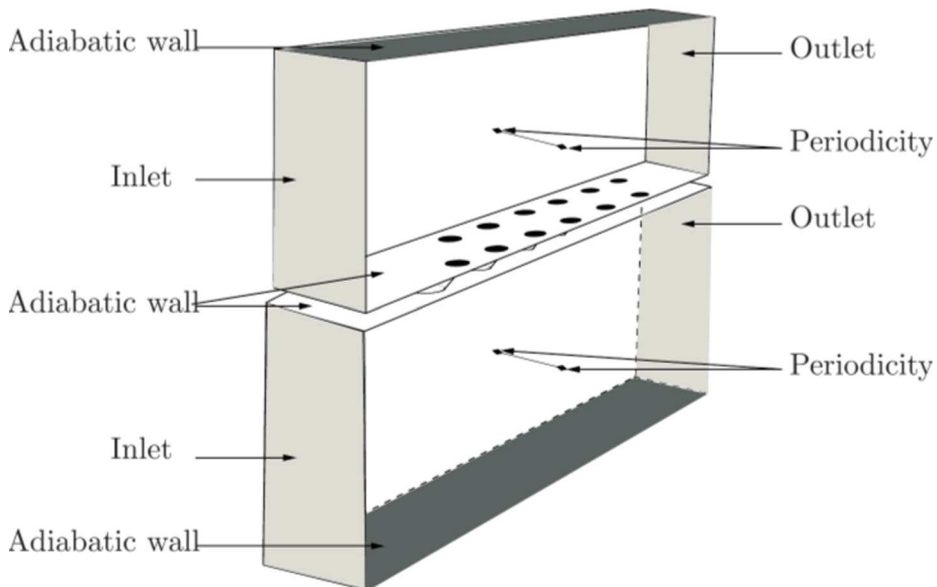


Fig. 5 Setup and boundary conditions of the fully resolved simulation

Table 1 Characteristics of the meshes. The last entries denote the mesh size of the multiperforated plate on the injection side in wall units

Case	R	Cells	Γ	σ_n	y^+
Coarse	0.5	14 284	6	0.041	112
Medium	2	858 459	1.5	0.48	29
Fine	4	6 705 379	1	0.91	14
Very fine	16	31 982 977	1	1	4
Reference	16	51 077 506	N/A	N/A	4

and since the RMS field [19] is quiet complex in terms of profile, it can not be imposed with only few cells.

In the following section the test case used to evaluate the model when increasing mesh resolution is described.

3 Description of the Validation Test Case

The homogeneous model of Mendez and Nicoud [16] has been validated on the LARA experiment [24], which is an upscaled version of a real multiperforated plate in which holes have a diameter of 5 mm. The present test case, Maveric-H, uses a more realistic hole diameter of 0.4 mm and a porosity σ of 0.04 typical of a helicopter effusion plate [25]. It is based on the Maveric experiment studied in [24, 26, 27] which consists of two parallel channels communicating through 144 holes. Thanks to the periodicity of the setup, only 12 holes can be computed as shown on Fig. 5. When using homogeneous and thickened-hole models, the apertures do not belong to the computational domain, and it was chosen to compute only the injection side. In this case, the mass flux imposed by the models is extracted from a the fully resolved simulation performed on the geometry presented on Fig. 5.

To test the present model, four meshes corresponding to four values of the R ratio with a uniform spatial resolution are considered, see Table 1. For the coarse, medium and fine meshes, simulations are carried out with both the homogeneous and the thickened-hole models. On the very fine mesh only the thickened-hole method is tested. A reference simulation where holes are resolved and taking both sides of the multiperforated plate is added for validation purposes. In the following section averaged and instantaneous results for various R resolutions are analysed in order to validate the new model.

4 Numerical Predictions

Time averaged solutions are first considered. To provide a fair comparison between homogeneous and thickened-hole models, the profiles are averaged over the transverse direction

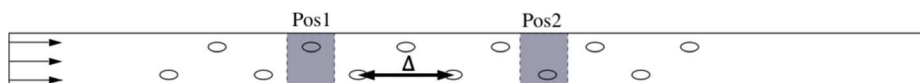


Fig. 6 Top view of the plate with the location of the averaging areas Pos1 and Pos2

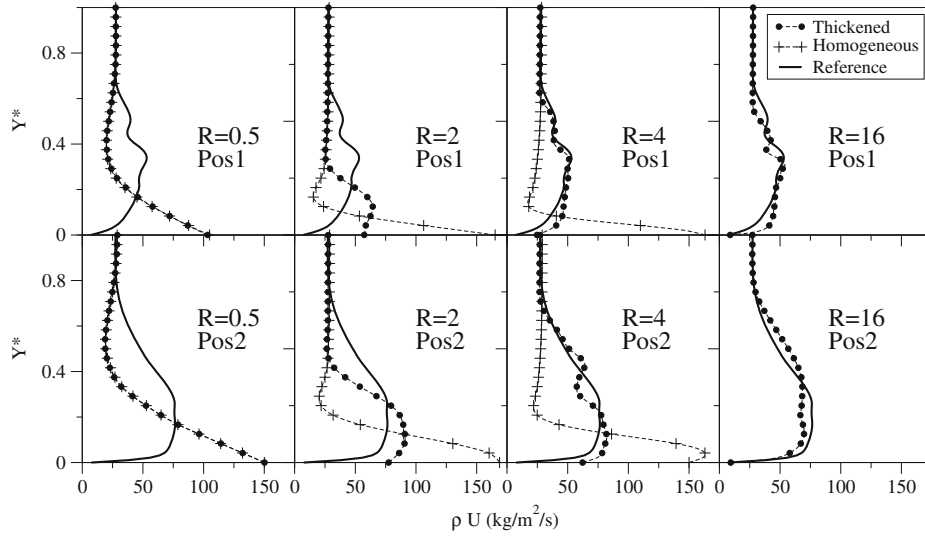


Fig. 7 Spatially and temporally averaged streamwise momentum ρU at positions Pos1 (top) and Pos2 (bottom), for ratios $R = 0.5; 2; 4; 16$ (from left to right). —: reference, •: thickened-hole model, +: homogeneous model

in two portions of the flow: Pos1, where the flow is not established and Pos2, (grey rectangles on Fig. 6), where the film cooling effect is present. Figures 7, 8 and 9 present profiles of momentum in the tangential direction, momentum in the normal direction and temperature, respectively, as a function of Y^* , the distance from the plate in the normal direction

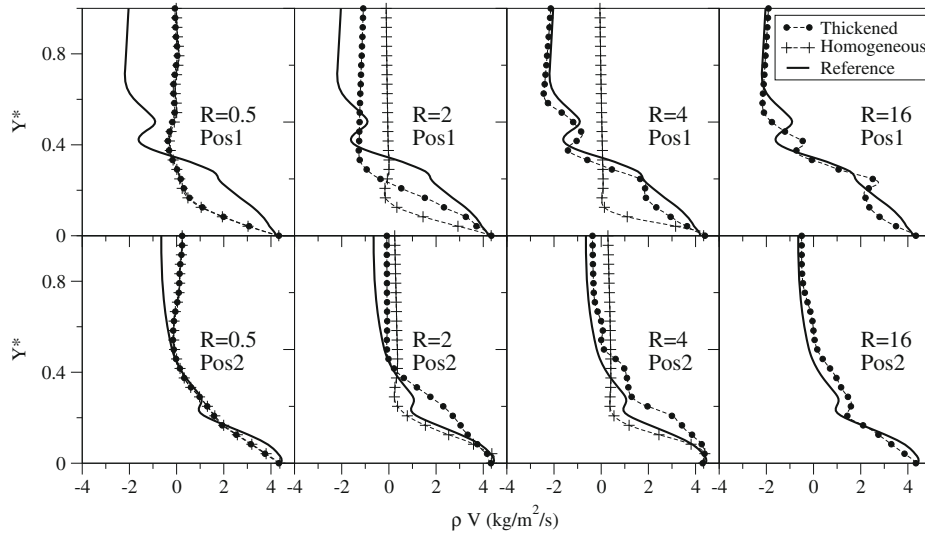


Fig. 8 Spatially and temporally averaged normal momentum ρV at positions Pos1 (top) and Pos2 (bottom), for ratios $R = 0.5; 2; 4; 16$ (from left to right). —: reference, •: thickened-hole model, +: homogeneous model

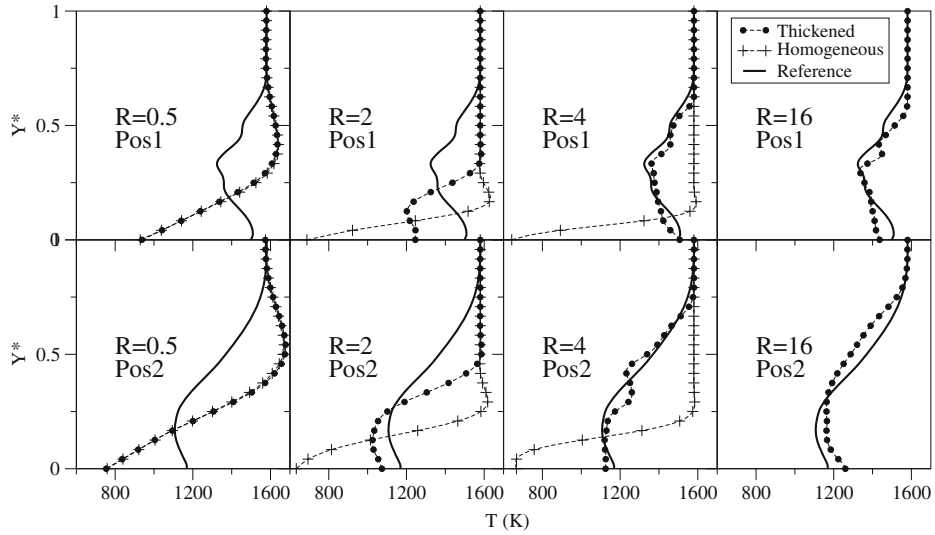


Fig. 9 Spatially and temporally averaged temperature profiles at positions Pos1 (top) and Pos2 (bottom), for ratios $R = 0.5; 2; 4; 16$ (from left to right). —: reference, •: thickened-hole model, +: homogeneous model

normalized by Δ the inter-row distance, Fig. 6. On Figs. 10 and 11, profiles for temperature RMS fluctuations as well as streamwise velocity RMS fluctuations are also presented.

When the ratio R is lower than one, the homogeneous and thickened-hole model give, as expected, very similar results, in bad agreement with the resolved computation. Figure 7 shows that the tangential momentum is too large close to the plate leading to a thinner

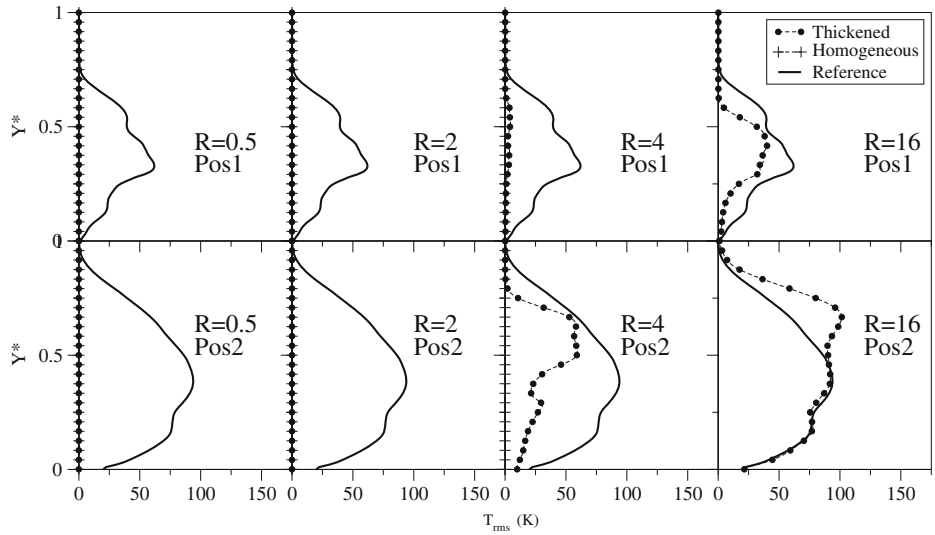


Fig. 10 Spatially and temporally averaged RMS temperature profiles at positions Pos1 (top) and Pos2 (bottom), for ratios $R = 0.5; 2; 4; 16$ (from left to right). —: reference, •: thickened-hole model, +: homogeneous model

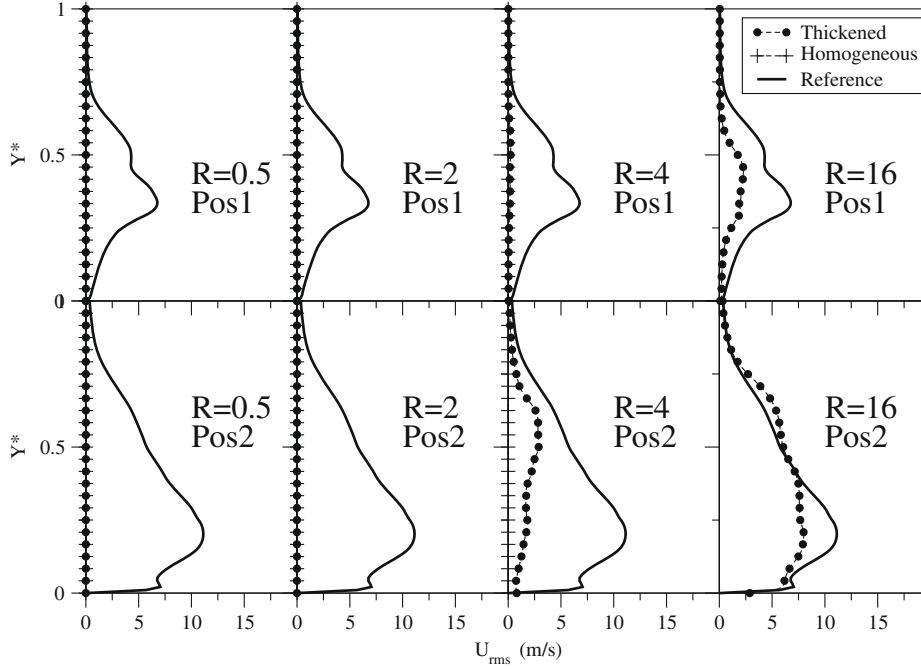


Fig. 11 Spatially and temporally averaged streamwise RMS velocity profiles at positions Pos1 (top) and Pos2 (bottom), for ratios $R = 0.5; 2; 4; 16$ (from left to right). —: reference, ●: thickened-hole model, +: homogeneous model

mixing layer and to a lower temperature at the wall as shown on Fig. 9. When the flow is established (Pos2), normal momentum is well represented since the mass flow rate through the multiperforated plate is correctly imposed (see Fig. 8).

When R is equal or bigger to 4, the thickened-hole model gives better results than the homogeneous model. With this resolution, results are close to the fully resolved one whatever the position and for all variables.

For intermediate values, $R = 2$, the thickened-hole model better predicts the evolution of the flow compared to the homogeneous model. Indeed, the shape of the mixing layer is accurately predicted both for established (Pos2) and non-established (Pos1) flows. In the non-established region, the thickened-hole model is able to capture the negative values for ρV observed in the resolved computation for $Y^* > 0.4$ (Fig. 8). This specific feature is crucial if one focuses on non-established flows.

RMS temperature fluctuations (Fig. 10) and streamwise RMS velocity fluctuations (Fig. 11) are produced when R is greater or equal to 4 with the thickened-hole model. For $R = 4$, the model predicts very small fluctuations at the first position (Pos1) where the film cooling is not established; the agreement being much better for Pos2 which points to potential issues when facing non fully established flows. Note that this specific difficulty can not be adequately treated with existing models other than the thickened-hole model. When $R = 16$, the RMS fluctuations match the reference data even in the non established region.

At this point, the thickened-hole model has been validated based solely on time and space averaged fields. The discrete form of this model however also allows to represent the flow fluctuations in LES as hinted by Figs. 11 and 10. This capacity is further illustrated by

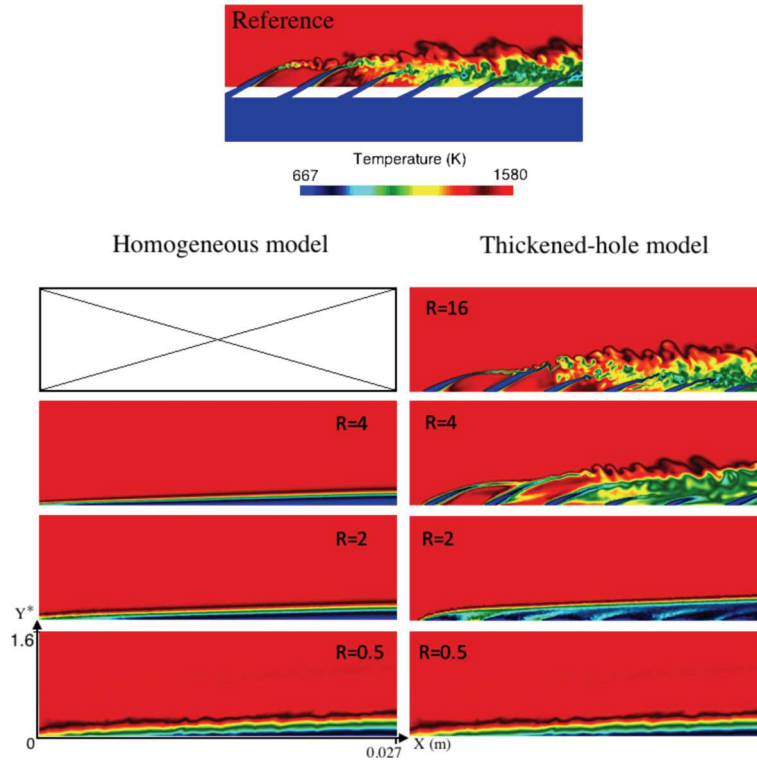


Fig. 12 Visualisation of the coolant film. Comparison between simulations using homogeneous model (left) and thickened-hole model (right) for various R values

Fig. 12 where instantaneous temperature fields for the homogeneous and the thickened-hole models for various R values are compared to the resolved simulation. With the thickened-hole model, jets can be distinguished for $R \geq 2$. This is a major step forward as the interaction between jets can now be examined. Furthermore, for $R \geq 4$, the jets are very similar to the resolved ones.

Note that results are presented for a uniform mesh resolution since it is the most general case with mesh used by academic and industry. However, the model is local (the cell size is taken from the mesh, not as an input parameter) and react to the local variation of wall resolution. Mesh variations could indeed have effects on the global result of a multiperforated plate. To enhance predictions, automatic mesh adaption could be envisioned so as to refine near jet wakes while coarsening between jets.

5 Conclusion

A heterogeneous thickened-hole approach has been introduced. Compared to a homogeneous model, it benefits from increasing mesh resolution. For high resolutions (large aperture-to-mesh ratio, $R > 2$, say), the thickened-hole model outperforms the homogeneous model [19]. Moreover, the solution converges to the one obtained with a fully resolved

computation when R is further increased. At the opposite, for small to moderate aperture-to-mesh ratio, the model proposed degenerates to a homogeneous model which is the best method for coarse meshes.

This new method allows a huge design process enhancement compared to a resolved simulation where holes are meshed. Indeed, with the thickened-hole model, from a unique mesh of an engine, many hole layouts can be tested: "One mesh fits all". This methodology was recently used in the design of a real engines [28–30].

Compliance with Ethical Standards

Conflict of interests The authors declare that they have no conflict of interest.

Publisher's Note Springer Nature remains neutral with regard to jurisdictional claims in published maps and institutional affiliations.

References

1. Schulz, A.: Combustor liner cooling technology in scope of reduced pollutant formation and rising thermal efficiencies. *Ann. N. Y. Acad. Sci.* **934**(1), 135–146 (2001)
2. Rizk, N., Mongia, H.: Low NOx rich-lean combustion concept application. AIAA paper (91-1962) (1991)
3. Goldstein, R.J.: Film cooling. *Adv. Heat Tran.* **7**, 321–379 (1971)
4. Lefebvre, A.H.: *Gas Turbines Combustion*. Taylor & Francis, New York (1999)
5. Poprawe, R., Kelbassa, I., Walther, K., Witty, M., Bohn, D., Krewinkel, R.: Optimising and manufacturing a laser-drilled cooling hole geometry for effusion-cooled multi-layer plates. Proc. of ISROMAC-12, Paper (20091) (2008)
6. Mayle, R.E., Camarata, F.J.: Multihole cooling effectiveness and heat transfer. *J. Heat Transf.* **97**, 534–538 (1975)
7. Pietrzyk, J.R., Bogard, D.G., Crawford, M.E.: Hydrodynamic measurements of jets in crossflow for gas turbine film cooling applications. *J. Turbomach.* **111**, 139–145 (1989)
8. Sinha, A.K., Bogard, D.G., Crawford, M.E.: Film-cooling effectiveness downstream of a single row of holes with variable density ratio. *J. Turbomach.* **113**, 442–449 (1991)
9. Crawford, M.E., Kays, W.M., Moffat, R.J.: Full-coverage film cooling. part I: comparison of heat transfer data for three injection angles. *J. Eng. Gas Turbines Power* **102**, 1000–1005 (1980)
10. Hale, C.A., Plesniak, M.W., Ramadhyani, S.: Film cooling effectiveness for short film cooling holes fed by a narrow plenum. *J. Turbomach.* **122**, 553–557 (2000)
11. LeBrocq, P.V., Launder, B.E., Priddin, C.H.: Discrete hole injection as a means of transpiration cooling; an experimental study. *Proc. Inst. Mech. Eng.* **187**(17), 149–157 (1973)
12. Metzger, D.E., Takeuchi, D.I., Kuenstler, P.A.: Effectiveness and heat transfer with full-coverage film-cooling. ASME Paper 73-GT-18 (1973)
13. Briones, A.M., Rankin, B.A., Stouffer, S.D., Erdmann, T.J., Burrus, D.L.: Parallelized, automated, and predictive imprint cooling model for combustion systems. *J. Eng. Gas Turbines Power* **139**(3), 031505 (2017)
14. Burdet, A., Abhari, R.S., Rose, M.G.: Modeling of film cooling—Part II model for use in three-dimensional computational fluid dynamics. *J. Turbomach.* **129**(2), 221–231 (2007)
15. Mazzei, L., Mazzei, L., Andreini, A., Andreini, A., Facchini, B., Facchini, B.: Assessment of modelling strategies for film cooling. *Int. J. Numer. Methods Heat Fluid Flow* **27**(5), 1118–1127 (2017)
16. Mendez, S., Nicoud, F.: Adiabatic homogeneous model for flow around a multiperforated plate. *AIAA J.* **46**(10), 2623–2633 (2008)
17. Rida, S., Reynolds, R., Chakraborty, S., Gupta, K.: Imprinted effusion modeling and dynamic cd calculation in gas turbine combustors. ASME Paper No GT2012-68804 (2012)
18. Voigt, S., Noll, B., Aigner, M.: Development of a macroscopic CFD model for effusion cooling applications. ASME Paper No GT2012-68251 (2012)
19. Mendez, S., Nicoud, F.: Large-eddy simulation of a bi-periodic turbulent flow with effusion. *J. Fluid Mech.* **598**, 27–65 (2008)

20. Most, A., Savary, N., Bérat, C.: Reactive flow modelling of a combustion chamber with a multiperforated liner. AIAA Paper (2007–5003) (2007)
21. Lahbib, D.: Modélisation Aérodynamique et Thermique des Multiperforations en LES. PhD thesis, Université Montpellier II (2015)
22. Koupper, C., Gicquel, L., Duchaine, F., Bonneau, G.: Advanced combustor exit plane temperature diagnostics based on large eddy simulations. *Flow Turbul. Combust.* **95**(1), 79–96 (2015)
23. Jaegle, F., Cabrit, O., Mendez, S., Poinso, T.: Implementation methods of wall functions in cell-vertex numerical solvers. *Flow Turbul. Combust.* **85**(2), 245–272 (2010)
24. Miron, P.: Étude Expérimentale des Lois de Parois et du Film de Refroidissement Produit par une Zone Multiperforée sur une Paroi Plane. PhD thesis, Université de Pau et des Pays de l'Adour (2005)
25. Florenciano, J.-L., Bruel, P.: LES fluid–solid coupled calculations for the assessment of heat transfer coefficient correlations over multi-perforated walls. *Aerosp. Sci. Technol.* **53**, 61–73 (2016)
26. Florenciano, J.: Etude de la Réponse d'un Écoulement Avec Transfert Pariétal de Masse à un Forçage Acoustique. PhD thesis, Université de Pau (2013)
27. Petre, B., Dorignac, E., Vullierme, J.J.: Study of the influence of the number of holes rows on the convective heat transfer in the case of full coverage film cooling. *Int. J. Heat Mass Transf.* **46**(18), 3477–3496 (2003)
28. Lamouroux, J., Richard, S., Malé, Q., Staffelbach, G., Dauplain, A., Misdariis, A.: On the combination of large eddy simulation and phenomenological soot modelling to calculate the smoke index from aero-engines over a large range of operating conditions. In: ASME Turbo Expo 2017: Turbomachinery Technical Conference and Exposition, pp. V04BT04A004–V04BT04A004. American Society of Mechanical Engineers (2017)
29. Thomas, M., Dauplain, A., Gicquel, L., Duchaine, F., Koupper, C., Nicoud, F.: Comparison of heterogeneous and homogeneous coolant injection models for large eddy simulation of multiperforated liners present in a combustion simulator. ASME Paper No GT2017-64622 (2017)
30. Vignat, G., Taliercio, G., Lamouroux, J., Da Veiga, S., Savary, N., Duchaine, P.: Analysis of performance sensitivity to geometrical variations of a modern helicopter engine combustor using les simulations. In: ASME Turbo Expo 2017: Turbomachinery Technical Conference and Exposition, pp. V04BT04A003–V04BT04A003. American Society of Mechanical Engineers (2017)